

# **Plasma-photocatalytic conversion of CO<sub>2</sub> at low temperatures:**

## **Understanding the synergistic effect of plasma-catalysis**

Danhua Mei<sup>a</sup>, Xinbo Zhu<sup>a</sup>, Chunfei Wu<sup>b,c</sup>, Bryony Ashford<sup>a</sup>, Paul T. Williams<sup>b</sup>, Xin Tu<sup>a,\*</sup>

<sup>a</sup> *Department of Electrical Engineering and Electronics, University of Liverpool, Liverpool, L69 3GJ, UK*

<sup>b</sup> *Energy & Resource Research Institute, University of Leeds, Leeds, LS2 9JT, UK*

<sup>c</sup> *School of Engineering, University of Hull, Hull, HU6 7RX, UK*

### **Corresponding Author**

\*Dr. Xin Tu

Department of Electrical Engineering and Electronics,

University of Liverpool,

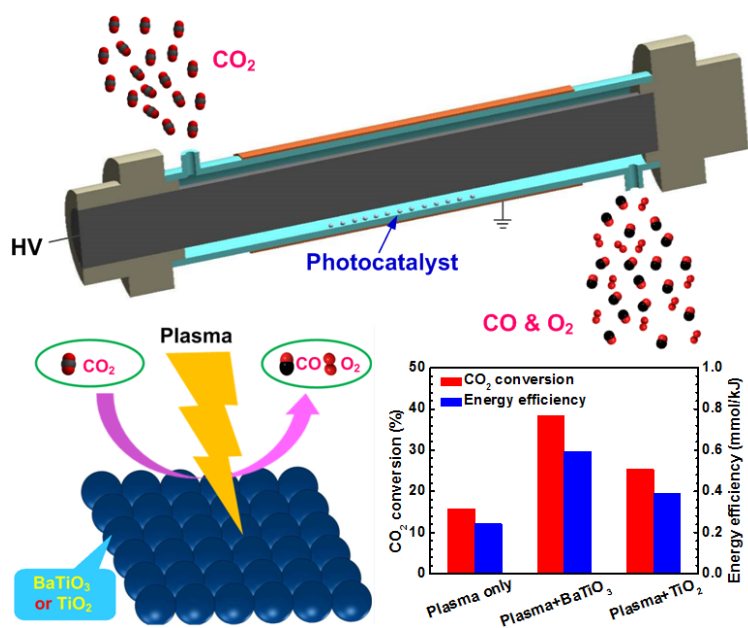
Liverpool, L69 3GJ,

UK

Tel: +44-1517944513

E-mail: xin.tu@liverpool.ac.uk

# Graphical abstract



1 **Abstract**

2 A coaxial dielectric barrier discharge (DBD) reactor has been developed for plasma-catalytic  
3 conversion of pure CO<sub>2</sub> into CO and O<sub>2</sub> at low temperatures (<150 °C) and atmospheric  
4 pressure. The effect of specific energy density (SED) on the performance of the plasma  
5 process has been investigated. In the absence of a catalyst in the plasma, the maximum  
6 conversion of CO<sub>2</sub> reaches 21.7 % at a SED of 80 kJ/L. The combination of plasma with  
7 BaTiO<sub>3</sub> and TiO<sub>2</sub> photocatalysts in the CO<sub>2</sub> DBD slightly increases the gas temperature of  
8 the plasma by 6-11 °C compared to the CO<sub>2</sub> discharge in the absence of a catalyst at a SED  
9 of 28 kJ/L. The synergistic effect from the combination of plasma with photocatalysts  
10 (BaTiO<sub>3</sub> and TiO<sub>2</sub>) at low temperatures contributes to a significant enhancement of both CO<sub>2</sub>  
11 conversion and energy efficiency by up to 250%. The UV intensity generated by the CO<sub>2</sub>  
12 discharge is significantly lower than that emitted from UV lamps that are used to activate  
13 photocatalysts in conventional photocatalytic reactions, which suggests that the UV  
14 emissions generated by the CO<sub>2</sub> DBD only play a very minor role in the activation of the  
15 BaTiO<sub>3</sub> and TiO<sub>2</sub> catalysts in the plasma-photocatalytic conversion of CO<sub>2</sub>. The synergy of  
16 plasma-catalysis for CO<sub>2</sub> conversion can be mainly attributed to the physical effect induced  
17 by the presence of catalyst pellets in the discharge and the dominant photocatalytic surface  
18 reaction driven by the plasma.

19

20 **Keywords:** Plasma-catalysis; dielectric barrier discharge; CO<sub>2</sub> conversion; synergistic effect;  
21 energy efficiency

22

## 23 1. Introduction

24 Recently, the abatement of carbon dioxide (CO<sub>2</sub>) has become a major global  
25 challenge as CO<sub>2</sub> is the main greenhouse gas and its emissions lead to the problems of  
26 climate change and global warming. Different strategies are being developed to tackle  
27 the challenges associated with CO<sub>2</sub> emissions, including carbon capture and storage  
28 (CCS), carbon capture and utilization (CCU), reducing fossil fuel consumption and  
29 boosting clean and renewable energy use. Direct conversion of CO<sub>2</sub> into value-added  
30 fuels and chemicals (e.g., CO, CH<sub>4</sub>, and methanol) offers an attractive route for  
31 efficient utilization of low value CO<sub>2</sub> whilst significantly reducing CO<sub>2</sub> emissions [1].  
32 However, CO<sub>2</sub> is a highly stable and non-combustible molecule, requiring  
33 considerable energy for upgrading and activation. Various synthetic approaches for  
34 CO<sub>2</sub> conversion have been explored, including solar driven photochemical reduction  
35 [2], electrochemical reduction [3] and thermal catalysis [4]. Despite their potential,  
36 further investigation into the development of cost-effective H<sub>2</sub> production methods,  
37 novel multifunctional catalysts and new catalytic processes are essential to improve  
38 the overall energy efficiency of CO<sub>2</sub> conversion processes and the product selectivity  
39 to practical and implementable levels.

40 Non-thermal plasma technology provides a promising alternative to the traditional  
41 catalytic route for the conversion of CO<sub>2</sub> into value-added fuels and chemicals at  
42 ambient conditions [5]. In non-thermal plasmas, highly energetic electrons and  
43 chemically reactive species (e.g., free radicals, excited atoms, ions, and molecules) can  
44 be generated for the initiation of both physical and chemical reactions. Non-thermal  
45 plasma has a distinct non-equilibrium character, which means the gas temperature in  
46 the plasma can be close to room temperature, whilst the electrons are highly energetic  
47 with a typical mean energy of 1-10 eV [6]. As a result, non-thermal plasma can easily

48 break most chemical bonds (e.g. C-O bonds), and enable thermodynamically  
49 unfavourable chemical reactions (e.g. CO<sub>2</sub> decomposition) to occur at ambient  
50 conditions. However, the use of plasma alone leads to low selectivity and yield  
51 towards the target end-products, and consequently causes low energy efficiency of the  
52 plasma processes. Recently, the combination of plasma with catalysis, known as  
53 plasma-catalysis, has attracted tremendous interest for environmental clean-up,  
54 greenhouse gas reforming, growth of carbon nanomaterials, ammonia synthesis and  
55 catalyst treatment [6-13]. The integration of plasma and solid catalysts has great  
56 potential to generate a synergistic effect, which can activate the catalysts at low  
57 temperatures and improve their activity and stability, resulting in the remarkable  
58 enhancement of reactant conversion, selectivity and yield of target products, as well as  
59 the energy efficiency of the plasma process [6]. Direct conversion of CO<sub>2</sub> into  
60 valuable CO and O<sub>2</sub> has been explored using different non-thermal plasmas [5, 14-25].  
61 However, most previous works have mainly focused on the conversion of CO<sub>2</sub> diluted  
62 with noble gases (e.g. He and Ar), which is not preferable from an industrial  
63 application point of view [14, 22, 25]. Further fundamental work is still required to  
64 optimize and improve the energy efficiency of the plasma process. In addition, finding  
65 a suitable and cost-effective catalyst for this reaction to enhance the overall efficiency  
66 of the process is a great challenge as very limited work has been focused on plasma-  
67 catalytic CO<sub>2</sub> conversion. A detailed understanding of the synergistic effect resulting  
68 from the combination of plasma and photocatalysts at low temperature is still required  
69 due to gaps in current knowledge resulting in only a vague idea of the interactions  
70 occurring. For example, it is not clear what the roles are of UV light and highly  
71 energetic electrons generated by the plasma in the plasma-photocatalytic chemical  
72 reactions.

73 In this work, a coaxial dielectric barrier discharge (DBD) has been developed for the  
74 plasma-photocatalytic conversion of pure CO<sub>2</sub> into CO and O<sub>2</sub> at low temperature. The effect  
75 of photocatalysts (BaTiO<sub>3</sub> and TiO<sub>2</sub>) on the temperatures (plasma gas temperature and the  
76 temperature on the catalyst surface) in the CO<sub>2</sub> DBD has been evaluated. The synergistic  
77 effect resulting from the combination of plasma and photocatalysts (BaTiO<sub>3</sub> and TiO<sub>2</sub>) has  
78 been investigated from both physical and chemical perspectives.

79

## 80 **2. Experimental**

81 In this study, a coaxial dielectric barrier discharge (DBD) reactor has been  
82 developed for the plasma-catalytic reduction of pure CO<sub>2</sub> into CO and O<sub>2</sub> at  
83 atmospheric pressure and low temperatures (< 150 °C), as shown in Fig. 1. An Al foil  
84 (ground electrode) was wrapped around the outside of a quartz tube with an external  
85 diameter of 22 mm and an inner diameter of 19 mm. A stainless steel tube with an  
86 outer diameter of 14 mm was used as the inner electrode (high voltage electrode). The  
87 discharge gap was fixed at 2.5 mm, whilst the discharge length was varied from 90 to  
88 150 mm. CO<sub>2</sub> was used as the feed gas without dilution at a flow rate of 15-60  
89 mL/min. The DBD reactor was supplied by an AC high voltage power supply with a  
90 peak-to-peak voltage of 10 kV and a frequency of 50 Hz. All the electrical signals  
91 were sampled by a four-channel digital oscilloscope (TDS2014). Different catalyst  
92 pellets BaTiO<sub>3</sub> (TCU) and TiO<sub>2</sub> (*Alfa Aesar*) with a diameter of 1 mm were packed  
93 into the discharge gap along the bottom of the quartz tube. Our previous work  
94 demonstrated that this packing method induces effective plasma-catalyst interactions,  
95 which might generate a synergistic effect and hence promote plasma-catalytic  
96 chemical reactions [6]. The gas temperature and the temperature on the surface of the  
97 catalysts in the DBD reactor was measured by a fiber optical temperature probe

98 (Omega, FOB102), which was placed in the plasma area. X-ray diffraction (XRD)  
 99 patterns of the fresh catalyst samples were recorded by a Siemens D5000  
 100 diffractometer using Cu-K $\alpha$  radiation in the  $2\theta$  range between 10° and 70°. X-ray  
 101 photoelectron spectroscopic (XPS) measurements were carried out on a Perkin-Elmer  
 102 PHI-5400 XPS system with mono-chromatic Mg K $\alpha$  (1253.6 eV) X-rays with a data  
 103 acquisition system. The spectra are referenced to C1s peak at 284.5 eV. The UV  
 104 intensity generated by the CO<sub>2</sub> DBD with and without a catalyst was measured by an  
 105 UV meter (Omega HHUVA1). The gas products were analyzed by a two-channel gas  
 106 chromatography (Shimadzu 2014) equipped with a flame ionization detector (FID) and  
 107 a thermal conductivity detector (TCD). The concentration of ozone was measured by  
 108 an ozone monitor (2B, Model 106-M). To evaluate the performance of the plasma  
 109 process, the specific energy density (SED), CO<sub>2</sub> conversion ( $C_{CO_2}$ ), selectivity  
 110 towards CO and O<sub>2</sub> ( $S_{CO}$  and  $S_{O_2}$ ), carbon and oxygen balance ( $B_{Carbon}$  and  $B_{Oxygen}$ ) as  
 111 well as energy efficiency ( $E$ ) are defined as follows:

$$112 \quad SED(kJ/L) = \frac{\text{Discharge power (kW)}}{\text{CO}_2 \text{ flow rate (L/s)}} \quad (1)$$

$$113 \quad C_{CO_2} (\%) = \frac{\text{CO}_2 \text{ converted (mol/s)}}{\text{CO}_2 \text{ input (mol/s)}} \times 100 \quad (2)$$

$$114 \quad S_{CO} (\%) = \frac{\text{CO produced (mol/s)}}{\text{CO}_2 \text{ converted (mol/s)}} \times 100 \quad (3)$$

$$115 \quad S_{O_2} (\%) = \frac{\text{O}_2 \text{ produced (mol/s)}}{\text{CO}_2 \text{ converted (mol/s)}} \times 100 \quad (4)$$

$$116 \quad B_{Carbon} (\%) = \frac{\text{CO}_2 \text{ unconverted (mol/s)} + \text{CO produced (mol/s)}}{\text{CO}_2 \text{ input (mol/s)}} \times 100 \quad (5)$$

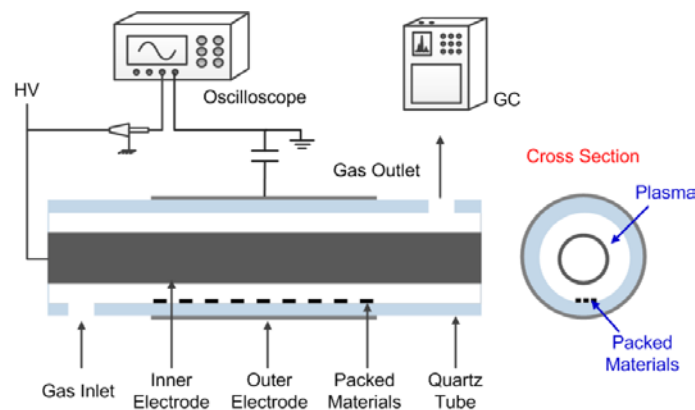
117

$$B_{\text{Oxygen}} (\%) = \frac{2 \times \text{CO}_2 \text{ unconverted (mol/s)} + \text{CO produced (mol/s)} + 2 \times \text{O}_2 \text{ produced (mol/s)}}{2 \times \text{CO}_2 \text{ input (mol/s)}} \times 100 \quad (6)$$

119

$$E (\text{mmol/kJ}) = \frac{\text{CO}_2 \text{ converted (mmol/s)}}{\text{Discharge power (kW)}} \quad (7)$$

121



122

123 Fig. 1. Schematic diagram of the experimental setup

124

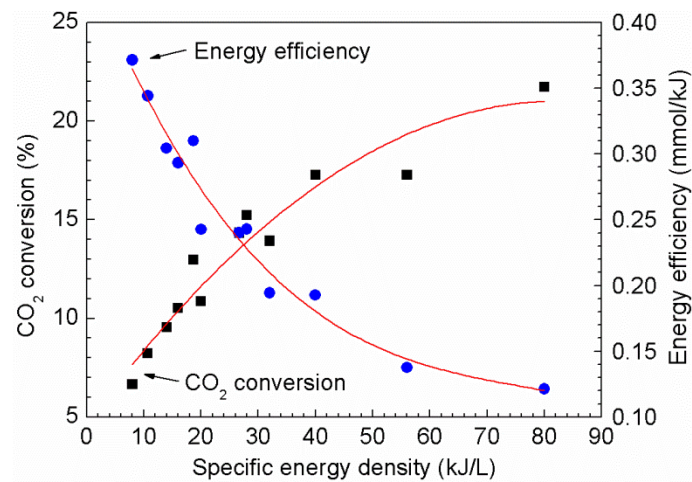
### 125 3. Results and Discussion

#### 126 3.1. Plasma-assisted conversion of CO<sub>2</sub> without catalyst

127 Fig. 2 shows the effect of specific energy density (SED) on the conversion of CO<sub>2</sub> and the  
128 energy efficiency of the plasma reaction in the absence of a catalyst. Clearly, increasing the  
129 specific energy density significantly enhances CO<sub>2</sub> conversion due to the increase in energy  
130 input to the discharge. The conversion of CO<sub>2</sub> is increased by a factor of 3 (from 6.7% to  
131 21.7%) as the SED rises from 8 kJ/L to 80 kJ/L. Similar conversion trends have been reported  
132 either using plasma alone or using plasma-catalysis for chemical reactions [26, 27]. Our  
133 previous works have shown that increasing energy input by changing applied voltage at a  
134 constant frequency could effectively increase the number of microdischarges and enhance the  
135 density of energetic electrons, as well as the gas temperature in the discharge [28-30], all of



136 which may contribute in different ways to the improvement in conversion. Moreover,  
 137 increasing the discharge power produces more chemically reactive species (e.g. O atoms),  
 138 which can further induce CO<sub>2</sub> dissociation to enhance its conversion. A lower feed gas flow  
 139 rate was reported to be beneficial for improving the conversion of reactants due to longer  
 140 retention time of the reactants in the plasma. In contrast, the specific energy density has an  
 141 opposite effect on the energy efficiency of the plasma process. Increasing the SED from 8  
 142 kJ/L to 80 kJ/L leads to a decrease of the energy efficiency from 0.37 mmol/kJ to 0.12  
 143 mmol/kJ, which is consistent with previous results [31]. In this work, the maximum energy  
 144 efficiency of 0.37 mmol/kJ is achieved at the lowest specific energy density of 8 kJ/L with a  
 145 discharge power of 8 W, a CO<sub>2</sub> feed flow rate of 60 mL/min and a discharge length of 150  
 146 mm.  
 147



148  
 149 Fig. 2. CO<sub>2</sub> conversion and energy efficiency as a function of SED

150  
 151 CO<sub>2</sub> dissociation by electron impact vibrational excitation (Eqs 8-9) is believed to be  
 152 the most effective pathway for CO<sub>2</sub> conversion in non-thermal plasmas, which can  
 153 lead to a high energy efficiency of more than 60% [32].





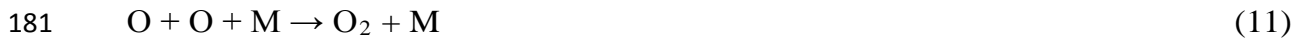
156 Where  $\nu^*$  is the vibrational excited state. Up to 97% of the total plasma energy can be  
157 transferred from electrons to vibrational excitation of  $\text{CO}_2$  if the plasma discharges  
158 have an electron temperature of 1-2 eV, or a reduced electric field ( $E/N$ ) of 20–40 Td  
159 [32]. Recent plasma modeling of  $\text{CO}_2$  splitting in a DBD reactor showed that in a  $\text{CO}_2$   
160 discharge with an average electron energy of 2-3 eV, only 12% of the energy can be  
161 allocated to vibrational states, whereas ~79% goes to electronic excited states, and ~4%  
162 and ~5% can be transferred to dissociation and ionization of  $\text{CO}_2$ , respectively [33].  
163 Their results showed that the majority (94%) of  $\text{CO}_2$  conversion is induced by  
164 reactions (e.g. dissociation) with ground state  $\text{CO}_2$  (shown in Eq. 10) and only 6% of  
165  $\text{CO}_2$  conversion occurs through reactions with vibrational excited  $\text{CO}_2$  at a high  
166 electric field [33].



168 In this study, the average electric field  $E$  in the  $\text{CO}_2$  DBD without a catalyst is  
169 estimated to be around 1.75 kV/mm under our experimental conditions, obtained from  
170 Lissajous figure [10], while the corresponding mean electron energy of the plasma is  
171 around 2.4 eV, calculated using BOLSIG+ code based on electron energy distribution  
172 function (EEDF) [34]. This result suggests that the electron impact dissociation of  
173  $\text{CO}_2$  might play a dominant role in  $\text{CO}_2$  conversion in this experiment.

174 The electron impact dissociation of  $\text{CO}_2$  in its vibrational excited states (Eq. 9) or  
175 ground state (Eq. 10) will most likely result in CO in its ground state ( $^1\Sigma$ ) and O atoms  
176 in both the ground state ( $^3P$ ) and metastable state ( $^1D$ ). However, since CO bands were  
177 observed in the emission spectra of the  $\text{CO}_2$  discharge generated in a similar coaxial  
178 DBD reactor, CO could also be formed in excited states [6].

179 Oxygen can be formed from the three-body recombination of atomic oxygen (Eq. 11)  
180 or from the reaction with a ground state CO<sub>2</sub> molecule (Eq. 12).



183 Oxygen might also be generated directly by electron impact dissociation of CO<sub>2</sub> if  
184 the electron has a high energy (> 15 eV).



186  
187 In this study, no carbon deposition is observed after the plasma conversion of CO<sub>2</sub>  
188 with and without catalyst. The main gas products from plasma conversion of pure CO<sub>2</sub>  
189 were CO and O<sub>2</sub>. The selectivities towards CO and O<sub>2</sub> are in the range of 91.5%-96.7%  
190 and 45.4%-48.5%, respectively, while the carbon balance (98.1%-99.5%) and oxygen  
191 balance (98.0%-99.6%) are very high. This agrees with recent experimental and  
192 modelling works in which CO and O<sub>2</sub> were identified as the main products in the  
193 conversion of CO<sub>2</sub> when using DBD [33, 35]. Ozone could be formed by the  
194 following reaction:



196 However, ozone was not detected in this work. Ozone could be decomposed by local  
197 heating generated by the plasma in the reactor. Andrev and co-workers suggested that  
198 oxygen formed from CO<sub>2</sub> dissociation could be initially converted into O<sub>3</sub>, followed  
199 by ozone decomposition into O<sub>2</sub> through electron impact reactions [36]. In contrast,  
200 recent plasma modelling of CO<sub>2</sub> conversion showed that the calculated fractional  
201 density of O<sub>3</sub> was only 0.05% in a similar DBD reactor [33]. In addition, the  
202 maximum rate for ozone formation in the DBD reactor was two orders of magnitude  
203 lower than that of the three-body recombination of atomic oxygen for O<sub>2</sub> production

204 [33]. It is worth noting that gas heating was not calculated explicitly in the model,  
205 which might be able to explain the difference in ozone formation in the experiment  
206 and modelling. Our previous study has shown the formation of CO and CO<sub>2</sub><sup>+</sup> spectra  
207 in a similar DBD containing CO<sub>2</sub> using optical emission spectroscopic diagnostics [6],  
208 which suggests electron impact ionization of CO<sub>2</sub> occurs in the plasma CO<sub>2</sub> reaction.



210 The recorded CO<sub>2</sub><sup>+</sup> spectra also reveal the formation of highly energetic electrons in the CO<sub>2</sub>  
211 discharge as the electron impact ionization of CO<sub>2</sub> requires electrons with a high energy of at  
212 least 13.8 eV.

213

### 214 **3.2. Plasma-photocatalytic conversion of CO<sub>2</sub>**

215 The effect of BaTiO<sub>3</sub> and TiO<sub>2</sub> photocatalysts on the conversion of CO<sub>2</sub> is shown in  
216 Fig. 3. It is clear that the presence of both BaTiO<sub>3</sub> and TiO<sub>2</sub> in the discharge  
217 significantly enhances the CO<sub>2</sub> conversion and energy efficiency of the plasma  
218 process. Packing BaTiO<sub>3</sub> pellets into the discharge gap exhibits exceptional  
219 performance with a remarkable enhancement of both CO<sub>2</sub> conversion (from 15.2% to  
220 38.3%) and energy efficiency (from 0.24 mmol/kJ to 0.60 mmol/kJ) by a factor of 2.5  
221 at a SED of 28 kJ/L.

222

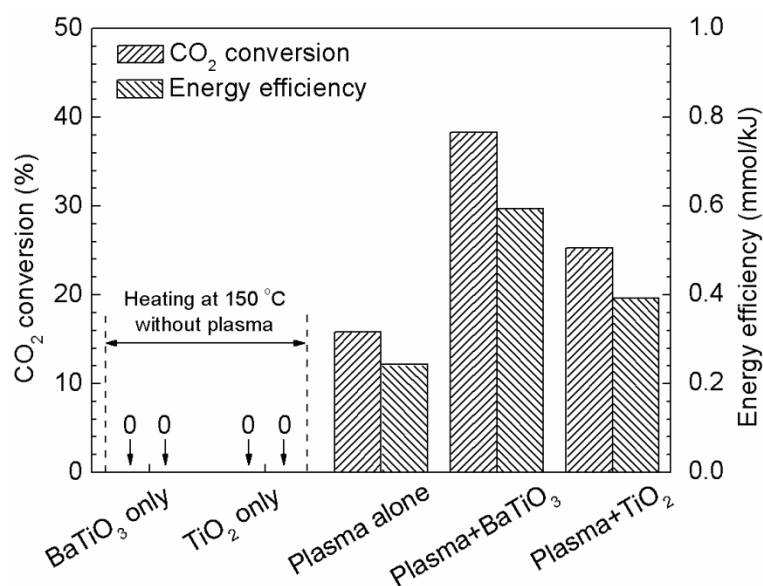


Fig. 3. Demonstration of the synergistic effect of plasma-catalysis for the conversion of CO<sub>2</sub> (SED = 28 kJ/L)

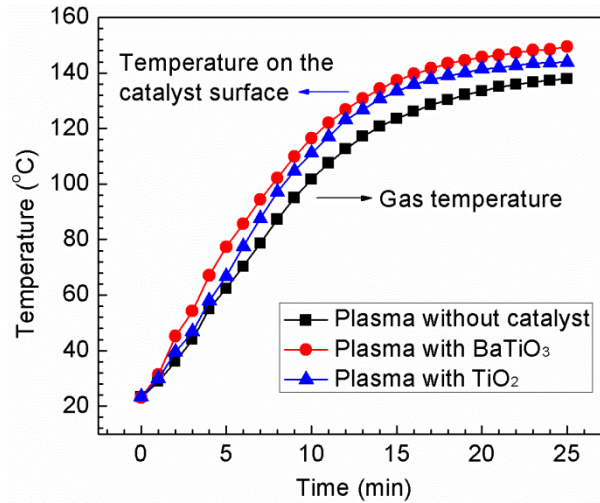
223  
224  
225  
226

The plasma gas temperature and the temperature on the catalyst surface in the plasma conversion of CO<sub>2</sub> have been measured in the DBD reactor at a SED of 28 kJ/L, as shown in Fig. 4. Clearly, the plasma gas temperature of the CO<sub>2</sub> DBD without a catalyst significantly increases from 23.3 °C to 123.5 °C in the first 15 min after igniting the plasma, after which it rises slowly and is almost constant (~138 °C) at 25 min when the plasma reaches a stable state. Similar evolution behaviour of the temperature can also be observed in the plasma-catalysis system (Fig. 4). In the CO<sub>2</sub> DBD reactor partially packed with the BaTiO<sub>3</sub> and TiO<sub>2</sub> catalysts, we note that the plasma temperature in the gas phase and the temperature on the catalyst surface are almost the same. Thus, only one temperature (the temperature on the catalyst surface) is shown in Fig.4 to present the temperature in the plasma-catalysis system. It is interesting to note that the combination of plasma with the BaTiO<sub>3</sub> and TiO<sub>2</sub> catalysts slightly increases the gas temperature (TiO<sub>2</sub>: ~144 °C and BaTiO<sub>3</sub>: ~149 °C) of the CO<sub>2</sub> discharge by 6-11 °C compared to the CO<sub>2</sub> DBD in the absence of a catalyst at

240

241 the same SED of 28 kJ/L. This phenomenon might be attributed to inelastic electron-  
242 molecule collisions in the plasma-catalytic processes [12, 37, 38].

243



244

245 Fig. 4. Plasma gas temperature and the temperature on the surface of BaTiO<sub>3</sub> and TiO<sub>2</sub>  
246 catalysts in the CO<sub>2</sub> DBD reactor (SED = 28 kJ/L). Note that the gas temperature of the CO<sub>2</sub>  
247 DBD and the temperature on the catalyst surface are almost the same when the catalyst  
248 (BaTiO<sub>3</sub> and TiO<sub>2</sub>) is placed in the plasma zone.

249

250 To understand the role of plasma in the reaction, a purely thermal experiment has  
251 been carried out by heating both photocatalysts in a pure CO<sub>2</sub> flow at 150 °C. No  
252 conversion and adsorption of CO<sub>2</sub> was observed. Thermodynamic equilibrium  
253 calculation of the CO<sub>2</sub> reaction has also confirmed that the conversion of CO<sub>2</sub> is  
254 almost zero at low temperatures (e.g., 150 °C), suggesting that an extremely low CO<sub>2</sub>  
255 conversion is expected from the thermal catalytic reduction of CO<sub>2</sub> when carried out at  
256 the same temperature as that used in the plasma reaction (see Fig. SI1 in the  
257 Supporting Information). The results clearly show that the exceptional reaction  
258 performance has been achieved by the use of plasma-catalysis, which is much higher

259 than the sum of plasma-alone and catalysis alone, indicating the formation of a  
260 synergistic effect when combining plasma with photocatalysts at low temperatures.

261 Catalysts can be integrated into a DBD system in different ways. The presence of the  
262 catalyst pellets in part of the gas gap still shows predominantly filamentary discharges  
263 and surface discharges on the catalyst surface, which induces effective interactions  
264 between plasma and catalyst for CO<sub>2</sub> activation. In this work, the dielectric constant of  
265 BaTiO<sub>3</sub> and TiO<sub>2</sub> is 10000 and 85, respectively. Previous experimental [39, 40] and  
266 simulation [41, 42] studies have shown that packing catalyst pellets, especially pellets  
267 with a high dielectric constant (e.g., BaTiO<sub>3</sub>), into the discharge gap can generate a  
268 non-uniform electric field with enhanced electric field strength near contact points  
269 between the pellets and the pellet-dielectric wall. The maximum local electric field  
270 near these contact points can be much higher than that in the void in a plasma-catalysis  
271 reactor, depending on the contact angle, curvature and dielectric constant of the  
272 materials [43]. The space (including the space filled with pellets) averaged electric  
273 field in a plasma fully packed with packing pellets is initially increased by a factor of  
274 1.4 when increasing the dielectric constant of the materials from 10 to 1000, above this  
275 the change in the electric field becomes negligible [43]. We have reported that the  
276 interaction of plasma and TiO<sub>2</sub> exhibited a strong effect on the electron energy  
277 distribution in the discharge with an increase in both highly energetic electrons and  
278 electric field [29]. This phenomenon can also be confirmed by previous work, showing  
279 that the presence of TiO<sub>2</sub> in a plasma leads to a significant increase of the reduced  
280 electric field [44]. These results suggest that the presence of the catalyst pellets in the  
281 plasma gap play a crucial role in inducing physical effects, such as enhancement of the  
282 electric field and production of more energetic electrons and reactive species, which in  
283 turn leads to chemical effects and contributes to the conversion of CO<sub>2</sub>. In this study,

284 the average electric field is increased by 9.0% and 10.9% with the presence of BaTiO<sub>3</sub>  
285 and TiO<sub>2</sub> in the discharge gap, respectively; whilst the corresponding mean electron  
286 energy is increased by 9.4% and 11.3% (see Fig. SI2 in the Supporting Information).  
287 Both of these effects contribute to the enhancement of the CO<sub>2</sub> conversion.

288 However, the enhancement of the reaction performance in terms of CO<sub>2</sub> conversion  
289 and energy efficiency is found to be more significant than only due to the changes in  
290 plasma physical parameters (e.g. average electric field). This suggests that in addition  
291 to the plasma physical effect and the resulting gas phase reactions (Eqs. 8-15), the  
292 contribution of a plasma-activated photocatalytic reaction to the synergy of plasma-  
293 catalysis cannot be ruled out. The XRD patterns of the samples show that BaTiO<sub>3</sub> has  
294 the tetragonal phase, while TiO<sub>2</sub> exhibits the crystal structure of anatase (see Fig. SI3  
295 in the Supporting Information). TiO<sub>2</sub> is a widely used photocatalyst with a wide band  
296 gap of 3.2 eV for anatase phase, while BaTiO<sub>3</sub> is a perovskite semiconductor  
297 photocatalyst with a band gap of 2.8-3.0 eV for tetragonal phase. It is well known that  
298 photocatalysts can be activated through the formation of electron-hole (e<sup>-</sup>-h<sup>+</sup>) pairs  
299 with the aid of sufficient photonic energy ( $h\nu$ ) with an appropriate wavelength to  
300 overcome the band-gap between the valence band and the conductive band [45]:

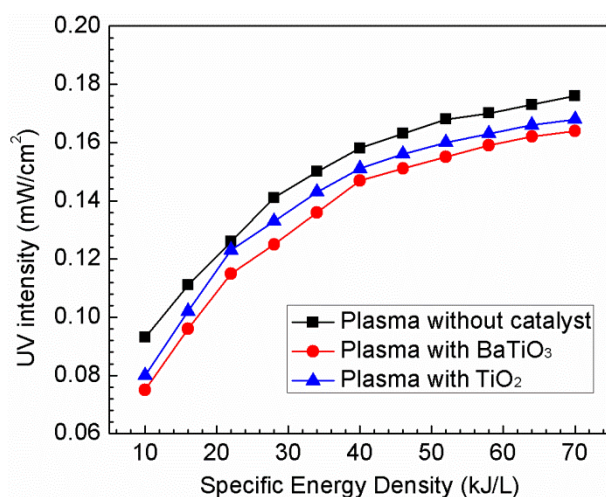


303 Plasma discharges can generate UV radiation without using any extra UV sources (e.g. UV  
304 lamps). This has been confirmed by the dominated N<sub>2</sub> (C-B) bands (between 300 nm and 400  
305 nm) in a CO<sub>2</sub> DBD in our previous work [6, 46]. However, UV radiation generated by  
306 plasma discharges is not always the controlling factor to activate photocatalysts due to its low  
307 intensity compared to that emitted by an UV lamp [47]. In this work, we have measured the  
308 UV intensity generated by the CO<sub>2</sub> DBD with and without a catalyst, as shown in Fig. 5. In



309 the absence of a catalyst in the DBD reactor, the UV intensity produced by the CO<sub>2</sub> discharge  
310 is about 0.141 mW/cm<sup>2</sup> at a SED of 28 kJ/L. When the BaTiO<sub>3</sub> and TiO<sub>2</sub> photocatalysts are  
311 placed in the plasma zone, the UV intensity of the CO<sub>2</sub> discharge is decreased to 0.115  
312 mW/cm<sup>2</sup> and 0.123 mW/cm<sup>2</sup>, respectively. Note that these values are significantly lower than  
313 the UV intensity (~20-60 mW/cm<sup>2</sup>) produced from UV lamps to activate photocatalysts in  
314 conventional photocatalytic reactions [48-50], which suggests that the UV emissions  
315 generated by the CO<sub>2</sub> discharge only play a minor role in the activation of the BaTiO<sub>3</sub> and  
316 TiO<sub>2</sub> photocatalysts. Similar results have been reported in the previous papers [51, 52].  
317 Assadi et al found that the UV light generated by a surface DBD was too weak to activate  
318 TiO<sub>2</sub> photocatalyst for the removal of 3-methylbutanal (3MBA) [51]. Sano et al reported that  
319 the UV intensity emitted by a N<sub>2</sub>/O<sub>2</sub> surface discharge was only 2.5 μW/cm<sup>2</sup> at an input  
320 power of 5 W. The contribution of the plasma UV activated photocatalytic reaction to the  
321 overall performance of acetaldehyde decomposition was less than 0.2% [52].

322



323

324 Fig. 5. UV intensity generated by the CO<sub>2</sub> DBD with and without a catalyst as a function of  
325 SED

326

327 Whitehead has suggested that electron-hole pairs can be created by electron impact  
328 upon the surface of photocatalysts since DBD can generate electrons of very similar  
329 energy (3 - 4 eV) to the photons [13, 53], as shown in Eqs. 18-19. Nakamura et al have  
330 also reported that photocatalysts can be activated by plasma and the electrons can be  
331 trapped onto the formed oxygen vacancies ( $V_o$ ) to enhance the photoexcitation process  
332 [54].

333 In this work, the exceptional performance of the plasma-catalytic  $CO_2$  conversion  
334 has been achieved through the combination of plasma and photocatalysts. However,  
335 the significant enhancement of the reaction performance in terms of  $CO_2$  conversion  
336 and energy efficiency cannot only be attributed to the changes in plasma physical  
337 parameters (e.g. increased average electric field), as the estimated average electric  
338 field and mean electron energy in the  $CO_2$  DBD are only increased by around 10%  
339 when the  $BaTiO_3$  and  $TiO_2$  catalysts are placed in the plasma zone. Furthermore, we  
340 find that the UV radiation generated by the  $CO_2$  DBD is significantly weak compared  
341 to that produced from UV lamps, which suggests that it might only play a minor role  
342 in the activation of photocatalytic  $CO_2$ , and its contribution to the exceptional  
343 performance of the plasma-catalytic reaction and the synergy of plasma-photocatalysis  
344 could be very weak or negligible. In this study, the highly energetic electrons  
345 generated by plasma are considered as the main driving force to activate the  
346 photocatalysts for  $CO_2$  conversion.



349 Previous investigation has shown that the photocatalytic conversion of  $CO_2$  is a  
350 multistep process, which involves the adsorption and subsequent activation of  $CO_2$   
351 molecules on the surface of photocatalysts and the subsequent dissociation of the C-O

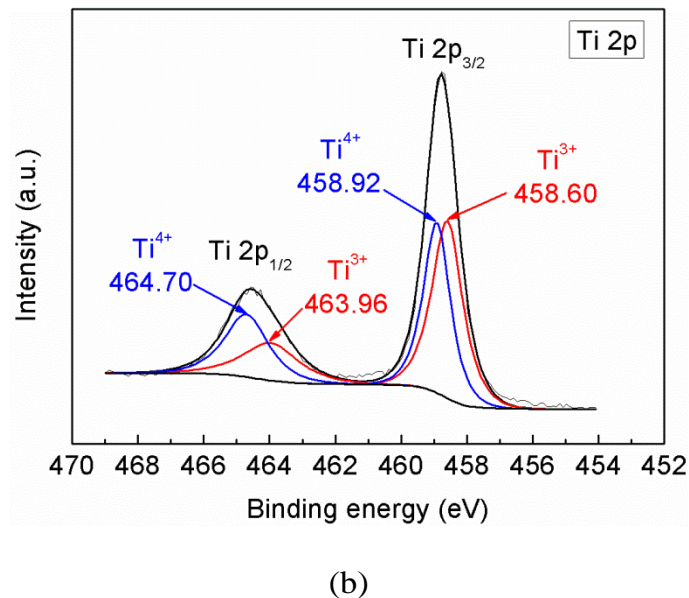
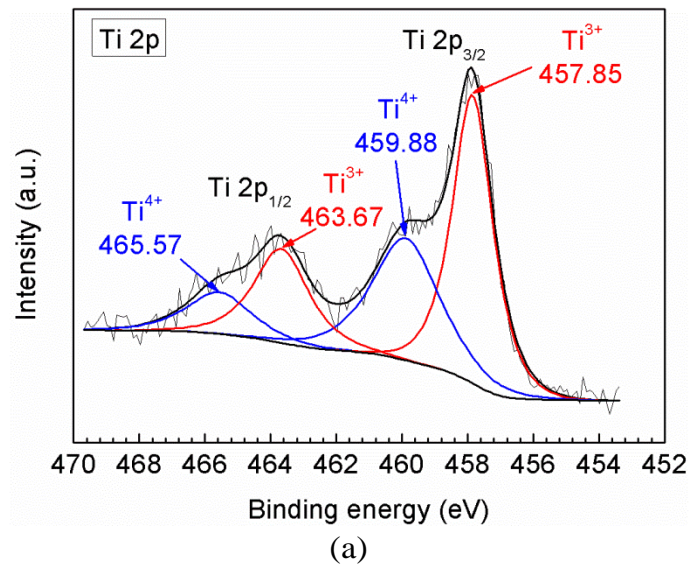
352 bond. The key step is the activation of CO<sub>2</sub> molecules through the transfer of trapped  
353 electrons to adsorbed CO<sub>2</sub> molecules in the V<sub>o</sub> [55].

354 However, the recombination rate of electron-hole pairs is 2 or 3 orders of magnitude  
355 faster than that of charge separation and transfer in a defect-free photocatalyst, which  
356 will limit the efficiency of CO<sub>2</sub> conversion [55]. The defect disorders in photocatalysts,  
357 such as V<sub>o</sub>, play an important role in the CO<sub>2</sub> reduction processes. V<sub>o</sub> has been  
358 considered as the active site for the adsorption and activation of reactants in a  
359 photocatalytic reaction [56]. In this study, XPS measurement has been performed to  
360 investigate the surface structure and element valence of the photocatalysts. Fig. 6(a)  
361 shows the deconvolution spectra of Ti 2p in the BaTiO<sub>3</sub> sample. Two components (Ti  
362 2p<sub>3/2</sub> and Ti 2p<sub>1/2</sub>) are identified and can be deconvoluted into 4 peaks. Two peaks at  
363 higher binding energy (459.88 and 465.57 eV) are assigned to the formal valence of Ti  
364 (4+) in BaTiO<sub>3</sub>; whilst the Ti 2p<sub>3/2</sub> and Ti 2p<sub>1/2</sub> peaks of Ti<sup>3+</sup> are located at around  
365 457.85 eV and 463.67 eV. The presence of Ti<sup>3+</sup> in the BaTiO<sub>3</sub> sample demonstrates  
366 the formation of V<sub>o</sub> on the catalyst surface through the following reaction [57, 58]:



368 where O<sup>2-</sup> is the lattice oxygen. Clearly, the formation of V<sub>o</sub> is followed by the change  
369 in the oxidative state of the vicinal Ti from Ti<sup>4+</sup> to Ti<sup>3+</sup> to retain the balance of local  
370 charge. Similarly, the Ti 2p<sub>3/2</sub> and Ti 2p<sub>1/2</sub> peaks of Ti<sup>3+</sup> can also be detected in the  
371 XPS profile of TiO<sub>2</sub>, as shown in Fig. 6(b). We find that there are more Ti<sup>3+</sup> species in  
372 the BaTiO<sub>3</sub> (60.9%) sample than in the TiO<sub>2</sub> (49.9%), which suggests more active  
373 sites (V<sub>o</sub>) were formed in the BaTiO<sub>3</sub> catalyst, resulting in the higher CO<sub>2</sub> conversion  
374 using the BaTiO<sub>3</sub> catalyst.

375

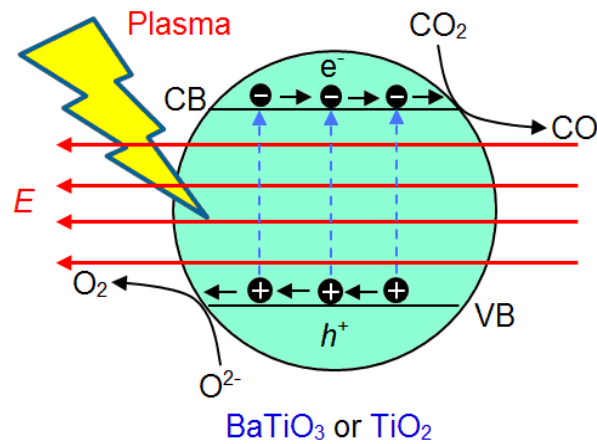
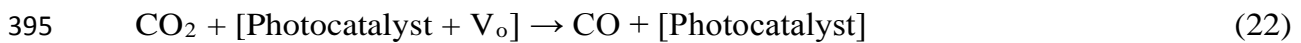


380 Fig. 6. XPS spectra of Ti 2p peaks for (a) BaTiO<sub>3</sub>; (b) TiO<sub>2</sub>

381

382 Moreover, the combination rate of electron-hole pairs can also be significantly  
 383 reduced in a plasma-photocatalytic system due to the presence of the electric field and  
 384 the interactions between the plasma and photocatalyst [59]. In this study, the process  
 385 of plasma-photocatalytic conversion of CO<sub>2</sub> can be described by Fig. 7. The electron  
 386 (e<sup>-</sup>) - hole (h<sup>+</sup>) pairs are generated with the aid of highly energetic electrons from the  
 387 gas discharge, and are moved in the opposite direction by the electric field, which can  
 388 reduce the probability of recombination. In the electron transfer process, CO<sub>2</sub>

389 adsorbed in the  $V_o$  is reduced to the anion radical  $CO_2^{\bullet-}$  by electrons from  $e^-$ - $h^+$  pairs  
 390 (Eq.21), followed by the decomposition of  $CO_2^{\bullet-}$  into CO and the occupation of one  
 391 oxygen atom in the  $V_o$  site. The overall reaction is expressed in Eq.22 [55, 60], in  
 392 which [Photocatalyst +  $V_o$ ] and [Photocatalyst] represent the defective and defect-free  
 393 photocatalysts, respectively.



398  
 399 Fig. 7. Reaction mechanisms of plasma-photocatalytic conversion of  $CO_2$  on the  
 400 surface of photocatalysts  
 401

402 In addition,  $V_o$  can be regenerated by oxidizing the surface  $O^{2-}$  anions using holes,  
 403 followed by releasing  $O_2$ , as shown in Eq. 23. To balance the charge, the  $Ti^{4+}$  in the  
 404 vicinity of the regenerated  $V_o$  can be reduced to  $Ti^{3+}$  by electrons [55, 61, 62], as  
 405 shown in Eq. 24. This cyclic healed-regeneration of the oxygen vacancies maintains  
 406 the equilibrium of the active sites in the photocatalysts and controls the conversion of  
 407  $CO_2$ , which can be confirmed by our experimental results as the  $CO_2$  conversion did  
 408 not change significantly when the plasma discharge was on for nearly two hours.

409 Therefore, we find that the synergistic effect resulting from the integration of DBD  
410 and photocatalysis for CO<sub>2</sub> conversion at low temperatures (without extra heating) can  
411 be attributed to the physical effect induced by the presence of photocatalysts in the  
412 discharge and the dominant photocatalytic surface reaction driven by the discharge.

413

### 414 **3.3. Energy efficiency**

415 Fig. 8 shows a comparison of the energy efficiency for CO<sub>2</sub> conversion using  
416 different atmospheric pressure non-thermal plasmas. It is clear that the energy  
417 efficiency (0.60 mmol/kJ) of the plasma CO<sub>2</sub> conversion in the presence of  
418 photocatalysts (BaTiO<sub>3</sub>) in this work is much higher than most of the other plasma  
419 processes regardless of the catalyst used. As shown in Fig. 8, the maximum energy  
420 efficiency of 0.69 mmol/kJ was achieved when the pure CO<sub>2</sub> decomposition was  
421 performed in an AC gliding arc discharge at a feed flow rate of 1.31 L/min. However,  
422 the corresponding conversion of CO<sub>2</sub> in this process was only 15.1%, which is  
423 significantly lower than that (38.3%) obtained in this work. A balance between CO<sub>2</sub>  
424 conversion and energy efficiency in the plasma processing of CO<sub>2</sub> is significantly  
425 important for the development and deployment of an efficient and cost-effective  
426 plasma process for CO<sub>2</sub> conversion and utilization [17]. In this work, the combination  
427 of DBD and photocatalysts (BaTiO<sub>3</sub> and TiO<sub>2</sub>) leads to a significant enhancement in  
428 the CO<sub>2</sub> conversion and energy efficiency of the plasma process, as well as a balance  
429 between them. It is also interesting to note that the energy efficiency obtained in this  
430 work (DBD) is much higher than that of similar chemical reactions using a  
431 conventional packed bed DBD reactor where materials and/or catalysts are fully  
432 packed into the discharge gap [63]. In our previous works, we found that packing  
433 catalysts into the entire discharge zone led to a strong packed-bed effect and was

434 found to shift the discharge mode from a typical strong filamentary microdischarge  
435 across the gap to a combination of surface discharge and weak microdischarge due to a  
436 significant reduction in the discharge volume [6, 10, 64]. As a result, only limited  
437 surface discharge can be generated on part of the catalyst surface and spatially limited  
438 microdischarges generated in the void space between pellet-pellet and pellet-quartz  
439 wall [10, 40]. The formation of strong filamentary discharges in a DBD reactor  
440 without a catalyst is strongly suppressed when the solid catalysts are fully packed into  
441 the discharge gap. It is well known that a packed-bed effect can enhance the electric  
442 field in the plasma, which contributes to the enhancement of the reaction performance  
443 to some extent. However, such a significant transition in behaviour of the discharge  
444 mode induced by the strong packed bed effect (fully packed) could substantially  
445 reduce the performance of plasma-catalytic conversion or reforming processes for  
446 energy and fuel production, as catalysts placed in the plasma area cannot be fully  
447 interacted and activated by the spatially limited discharges and weak interactions  
448 between the plasma and catalyst [6, 10]. Our previous work has clearly shown that  
449 how to pack catalysts in a DBD reactor is of primary importance to induce strong  
450 physical and chemical interactions between the plasma and catalyst, which  
451 consequently affects the generation of the synergistic effect of the plasma-catalytic  
452 reaction, especially for the conversion of undiluted reactants to valuable fuels and  
453 chemicals [6].

454 One may argue that as packed-bed DBD reactors have been demonstrated to be  
455 effective at removing a wide range of low concentration (10-1000 ppm) environmental  
456 gas pollutants [43], they could also be beneficial in the conversion of undiluted  
457 reactants. However, the major reaction mechanisms involved in the removal of dilute  
458 and low concentration gas pollutants and in the conversion of undiluted reactants (e.g.

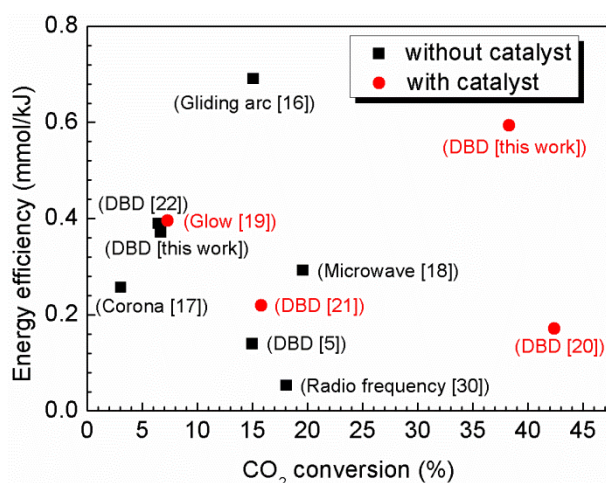
459 CO<sub>2</sub> or a mixture of CO<sub>2</sub> and CH<sub>4</sub>) are significantly different due to different  
460 concentrations of reactants in the plasma chemical reactions. In the former reactions,  
461 highly energetic electrons mainly collide with carrier gas (e.g. air) to generate  
462 chemically reactive species (e.g. O, O<sub>3</sub>, OH and N<sub>2</sub> (A)) which play dominant roles in  
463 the stepwise decomposition and oxidation of low concentration (ppm level) pollutants  
464 into CO, CO<sub>2</sub>, H<sub>2</sub>O and other by-products [65]. In contrast, electron impact reactions  
465 with reactants (e.g. CO<sub>2</sub>) make significant contributions to the conversion of undiluted  
466 reactants in the latter reactions as carrier gases (e.g. N<sub>2</sub> and Ar) are not preferable. The  
467 transition behaviour of the discharge mode resulting in weak interactions of plasma  
468 and catalyst induced by the packed bed effect might not be so important in the former  
469 reactions since the increased electric field in the packed bed DBD reactor might be  
470 sufficient to produce reactive species for the removal of pollutants of ppm level. In  
471 addition, even a catalyst support (e.g.  $\gamma$ -Al<sub>2</sub>O<sub>3</sub> and SiO<sub>2</sub>) placed in a packed bed DBD  
472 reactor could absorb or decompose some gas pollutants of low concentration [66, 67],  
473 leading us to think that the negative effect caused by the weak interaction between the  
474 plasma and packing catalysts (or supports) might be insignificant in the removal of  
475 dilute gas pollutants.

476 Further improvement in the energy efficiency of this process can be expected from  
477 the optimization of the plasma power and the design of new catalysts (e.g. coating  
478 metal nanoparticles on the photocatalysts). For example, previous simulation work has  
479 suggested that the energy efficiency of a plasma reactor can be enhanced by a factor of  
480 4 when using rectangular pulses instead of a sinusoidal voltage [68].

481 The high reaction rate and fast attainment of steady state in plasma processes allow  
482 rapid start-up and shutdown of the process compared to thermal treatment, whilst  
483 plasma systems can also work efficiently with a rather small and compact size. This



484 offers flexibility for plasma-catalytic processes to be integrated with renewable energy  
 485 sources such as waste energy from wind power, as the surplus energy could provide  
 486 cheap waste electricity for powering the plasma-catalytic process, making it more  
 487 effective in reducing CO<sub>2</sub> emissions.  
 488



489  
 490 Fig. 8. Comparison of energy efficiency for CO<sub>2</sub> conversion with different  
 491 atmospheric pressure plasma processes  
 492

#### 493 4. Conclusions

494 In this study, plasma-photocatalytic conversion of CO<sub>2</sub> into CO and O<sub>2</sub> has been  
 495 investigated using a DBD reactor combined with BaTiO<sub>3</sub> and TiO<sub>2</sub> photocatalysts.  
 496 The combination of plasma with the BaTiO<sub>3</sub> and TiO<sub>2</sub> photocatalysts in the CO<sub>2</sub> DBD  
 497 slightly increases the gas temperature of the plasma by 6-11 °C compared to the CO<sub>2</sub>  
 498 discharge in the absence of a catalyst at a SED of 28 kJ/L, while the plasma gas  
 499 temperature in the gas phase is almost the same as the temperature on the surface of  
 500 the photocatalysts (BaTiO<sub>3</sub> and TiO<sub>2</sub>) in the plasma-catalytic DBD reactor. The  
 501 combination of plasma with BaTiO<sub>3</sub> and TiO<sub>2</sub> catalysts has shown a synergistic effect,  
 502 which significantly enhances the conversion of CO<sub>2</sub> and the energy efficiency by a

503 factor of 2.5 compared to the plasma reaction in the absence of a catalyst. The  
504 presence of the catalyst pellets in the plasma gap is found to play a dominant role in  
505 inducing plasma physical effects, such as the enhancement of the electric field and  
506 production of more energetic electrons and reactive species, which in turn leads to  
507 chemical effects and partly contributes to the conversion of CO<sub>2</sub>. We find that the  
508 intensity of UV emissions generated in the CO<sub>2</sub> DBD is significantly lower than that  
509 emitted from external UV sources (e.g. UV lamps) that are commonly used to activate  
510 photocatalysts in conventional photocatalytic reactions. This phenomenon suggests  
511 that the UV emissions generated by the CO<sub>2</sub> DBD only play a minor role in the  
512 activation of the BaTiO<sub>3</sub> and TiO<sub>2</sub> catalysts in the plasma-photocatalytic conversion  
513 of CO<sub>2</sub>, and its contribution to the achieved exceptional performance of the plasma-  
514 photocatalytic reaction and the synergy of plasma-photocatalysis could be very weak  
515 or negligible. In this study, the highly energetic electrons generated by plasma have  
516 been considered as the main driving force to activate the photocatalysts for CO<sub>2</sub>  
517 conversion. The overall synergistic effect resulting from the integration of DBD with  
518 photocatalysis for CO<sub>2</sub> conversion at low temperatures (without extra heating) can be  
519 attributed to both the physical effect induced by the presence of the catalyst in the  
520 discharge and the dominant photocatalytic surface reaction driven by energetic  
521 electrons from the CO<sub>2</sub> discharge.

522

### 523 **Acknowledgements**

524 Support of this work by the UK EPSRC is gratefully acknowledged.

### 525 **Appendix A. Supplementary material**

526 Electronic Supplementary Information (ESI) available: [details of thermodynamic  
527 equilibrium calculation of CO<sub>2</sub> conversion and XRD patterns of photocatalysts are available].

528

529 **References**

- 530 [1] N.A.M. Razali, K.T. Lee, S. Bhatia, A.R. Mohamed, *Renew. Sust. Energ. Rev.* 16  
531 (2012) 4951-4964.
- 532 [2] M. Tahir, N.S. Amin, *Renew. Sust. Energ. Rev.* 25 (2013) 560-579.
- 533 [3] N.S. Spinner, J.A. Vega, W.E. Mustain, *Catal. Sci. Technol.* 2 (2012) 19-28.
- 534 [4] R.W. Dorner, D.R. Hardy, F.W. Williams, H.D. Willauer, *Energ. Environ. Sci.* 3 (2010)  
535 884-890.
- 536 [5] S. Paulussen, B. Verheyde, X. Tu, C. De Bie, T. Martens, D. Petrovic, A. Bogaerts, B.  
537 Sels, *Plasma Sources Sci. Technol.* 19 (2010) 034015.
- 538 [6] X. Tu, J.C. Whitehead, *Appl. Catal. B-Environ.* 125 (2012) 439-448.
- 539 [7] H.L. Chen, H.M. Lee, S.H. Chen, M.B. Chang, S.J. Yu, S.N. Li, *Environ. Sci. Technol.*  
540 43 (2009) 2216-2227.
- 541 [8] H.L. Chen, H.M. Lee, S.H. Chen, Y. Chao, M.B. Chang, *Appl. Catal. B-Environ.* 85  
542 (2008) 1-9.
- 543 [9] E.C. Neyts, B. A, *J. Phys. D: Appl. Phys.* 47 (2014) 224010.
- 544 [10] X. Tu, H.J. Gallon, M.V. Twigg, P.A. Gorry, J.C. Whitehead, *J. Phys. D: Appl. Phys.*  
545 44 (2011) 274007.
- 546 [11] X. Tu, H.J. Gallon, J.C. Whitehead, *Catal. Today.* 211 (2013) 120-125.
- 547 [12] J. Van Durme, J. Dewulf, C. Leys, H. Van Langenhove, *Appl. Catal. B-Environ.* 78  
548 (2008) 324-333.
- 549 [13] J.C. Whitehead, *Pure Appl. Chem.* 82 (2010) 1329-1336.
- 550 [14] S.L. Brook, M. Marquez, S.L. Suib, Y. Hayashi, H. Matsumoto, *J. Catal.* 180 (1998)  
551 225-233.
- 552 [15] A. Indarto, J.-W. Choi, H. Lee, H.K. Song, *Environ. Eng. Sci.* 23 (2006) 1033-1043.

- 553 [16] A. Indarto, D.R. Yang, J.W. Choi, H. Lee, H.K. Song, *J. Hazard. Mater.* 146 (2007)  
554 309-315.
- 555 [17] T. Mikoviny, M. Kocan, S. Matejcik, N.J. Mason, J.D. Skalny, *J. Phys. D: Appl. Phys.*  
556 37 (2004) 64-73.
- 557 [18] M. Tsuji, T. Tanoue, K. Nakano, Y. Nishimura, *Chem. Lett.* (2001) 22-23.
- 558 [19] J.Y. Wang, G.G. Xia, A.M. Huang, S.L. Suib, Y. Hayashi, H. Matsumoto, *J. Catal.* 185  
559 (1999) 152-159.
- 560 [20] S. Wang, Y. Zhang, X. Liu, X. Wang, *Plasma Chem. Plasma Process.* 32 (2012) 979-  
561 989.
- 562 [21] Q.Q. Yu, M. Kong, T. Liu, J.H. Fei, X.M. Zheng, *Plasma Chem. Plasma Process.* 32  
563 (2012) 153-163.
- 564 [22] G.Y. Zheng, J.M. Jiang, Y.P. Wu, R.X. Zhang, H.Q. Hou, *Plasma Chem. Plasma*  
565 *Process.* 23 (2003) 59-68.
- 566 [23] D. Mei, Y.-L. He, S. Liu, J.D. Yan, X. Tu, *Plasma Process. Polym.* (2015) DOI:  
567 10.1002/ppap.201500159.
- 568 [24] R. Aerts, W. Somers, A. Bogaerts, *ChemSusChem.* 8 (2015) 702-716.
- 569 [25] M. Ramakers, I. Michielsen, R. Aerts, V. Meynen, A. Bogaerts, *Plasma Process. Polym.*  
570 12 (2015) 755-763.
- 571 [26] A. Baylet, P. Marecot, D. Duprez, X. Jeandel, K. Lombaert, J.M. Tatibouet, *Appl. Catal.*  
572 *B-Environ.* 113 (2012) 31-36.
- 573 [27] H.B. Zhang, K. Li, T.H. Sun, J.P. Jia, Z.Y. Lou, L.L. Feng, *Chem. Eng. J.* 241 (2014)  
574 92-102.
- 575 [28] R. Snoeckx, R. Aerts, X. Tu, A. Bogaerts, *J. Phys. Chem. C.* 117 (2013) 4957-4970.
- 576 [29] X. Tu, H.J. Gallon, J.C. Whitehead, *J. Phys. D: Appl. Phys.* 44 (2011) 482003.

- 577 [30] X. Tu, B. Verheyde, S. Corthals, S. Paulussen, B.F. Sels, *Phys. Plasmas*. 18 (2011)  
578 080702.
- 579 [31] L.F. Spencer, A.D. Gallimore, *Plasma Chem. Plasma Process.* 31 (2011) 79-89.
- 580 [32] A. Fridman, *Plasma Chemistry*, Cambridge University Press, New York, 2008.
- 581 [33] R. Aerts, T. Martens, A. Bogaerts, *J. Phys. Chem. C*. 116 (2012) 23257-23273.
- 582 [34] X.B. Zhu, X. Gao, C.H. Zheng, Z.H. Wang, M.J. Ni, X. Tu, *RSC Adv.* 4 (2014) 37796-  
583 37805.
- 584 [35] F. Brehmer, S. Welzel, M.C.M. van de Sanden, R. Engeln, *J. Appl. Phys.* 116 (2014)  
585 123303.
- 586 [36] I.A. Semiokhin, Y.P. Andreev, *Russ. J. Phys. Chem.*, 40 (1966) 1161.
- 587 [37] H.H. Kim, A. Ogata, S. Futamura, *IEEE Trans. Plasma Sci.* 34 (2006) 984-995.
- 588 [38] T. Hammer, T. Kappes, M. Baldauf, *Catal. Today*. 89 (2004) 5-14.
- 589 [39] H.J. Gallon, H.H. Kim, X. Tu, J.C. Whitehead, *IEEE Trans. Plasma Sci.* 39 (2011)  
590 2176-2177.
- 591 [40] X. Tu, H.J. Gallon, J.C. Whitehead, *IEEE Trans. Plasma Sci.* 39 (2011) 2172-2173.
- 592 [41] W.S. Kang, J.M. Park, Y. Kim, S.H. Hong, *IEEE Trans. Plasma Sci.* 31 (2003) 504-510.
- 593 [42] M. Zaka-ul-Islam, K. Van Laer, A. Bogaerts, 31th International Conference on  
594 Phenomena in Ionized Gases Granada, Spain, 2013.
- 595 [43] H.L. Chen, H.M. Lee, S.H. Chen, M.B. Chang, *Ind. Eng. Chem. Res.* 47 (2008) 2122-  
596 2130.
- 597 [44] O. Guaitella, L. Gatilova, A. Rousseau, *Appl. Phys. Lett.* 86 (2005) 151502.
- 598 [45] L.G. Devi, G. Krishnamurthy, *J. Phys. Chem. A*. 115 (2011) 460-469.
- 599 [46] C. Subrahmanyam, M. Magureanu, D. Laub, A. Renken, L. Kiwi-Minsker, *J. Phys.*  
600 *Chem. C*. 111 (2007) 4315-4318.

- 601 [47] O. Guaitella, F. Thevenet, E. Puzenat, C. Guillard, A. Rousseau, *Appl. Catal. B-*  
602 *Environ.* 80 (2008) 296-305.
- 603 [48] A. Cybula, M. Klein, A. Zaleska, *Appl. Catal. B-Environ.* 164 (2015) 433-442.
- 604 [49] S. Xie, Y. Wang, Q. Zhang, W. Deng, Y. Wang, *ACS Catal.* 4 (2014) 3644-3653.
- 605 [50] A.A. Assadi, A. Bouzaza, S. Merabet, D. Wolbert, *Chem. Eng. J.* 258 (2014) 119-127.
- 606 [51] A.A. Assadi, J. Palau, A. Bouzaza, J. Penya-Roja, V. Martinez-Soriac, D. Wolbert, J.  
607 *Photoch. Photobio. A.* 282 (2014) 1-8.
- 608 [52] T. Sano, N. Negishi, E. Sakai, S. Matsuzawa, *J. Mol. Catal. A-Chem.* 245 (2006) 235-  
609 241.
- 610 [53] A.E. Wallis, J.C. Whitehead, K. Zhang, *Catal. Lett.* 113 (2007) 29-33.
- 611 [54] I. Nakamura, N. Negishi, S. Kutsuna, T. Ihara, S. Sugihara, E. Takeuchi, *J. Mol. Catal.*  
612 *A-Chem.* 161 (2000) 205-212.
- 613 [55] L.J. Liu, Y. Li, *Aerosol Air Qual. Res.* 14 (2014) 453-469.
- 614 [56] X.Y. Pan, M.Q. Yang, X.Z. Fu, N. Zhang, Y.J. Xu, *Nanoscale*, 5 (2013) 3601-3614.
- 615 [57] N.A. Deskins, R. Rousseau, M. Dupuis, *J. Phys. Chem. C.* 115 (2011) 7562-7572.
- 616 [58] L.J. Liu, C.Y. Zhao, Y. Li, *J. Phys. Chem. C.* 116 (2012) 7904-7912.
- 617 [59] A. Mizuno, Y. Kisanuki, M. Noguchi, S. Katsura, S.H. Lee, U.K. Hong, S.Y. Shin, J.H.  
618 Kang, *IEEE Trans. Ind. Appl.* 35 (1999) 1284-1288.
- 619 [60] W. Pipornpong, R. Wanbayor, V. Ruangpornvisuti, *Appl. Surf. Sci.* 257 (2011) 10322-  
620 10328.
- 621 [61] L.B. Xiong, J.L. Li, B. Yang, Y. Yu, *J. Nanomater.* (2012) 831524.
- 622 [62] A. Fujishima, T.N. Rao, D.A. Tryk, *J. Photochem. Photobiol. C: Photochem. Rev.* 1  
623 (2000) 1-21.
- 624 [63] D.H. Mei, X.B. Zhu, Y.L. He, J.D. Yan, X. Tu, *Plasma Sources Sci. Technol.* 24 (2015)  
625 015011.

- 626 [64] H.J. Gallon, X. Tu, J.C. Whitehead, *Plasma Process. Polym.* 9 (2012) 90-97.
- 627 [65] X.B. Zhu, X. Gao, R. Qin, Y.X. Zeng, R.Y. Qu, C.H. Zheng, X. Tu, *Appl. Catal. B-*  
628 *Environ.* 170 (2015) 293-300.
- 629 [66] A.E. Wallis, J.C. Whitehead, K. Zhang, *Appl. Catal. B-Environ.* 74 (2007) 111-116.
- 630 [67] A.E. Wallis, J.C. Whitehead, K. Zhang, *Appl. Catal. B-Environ.* 72 (2007) 282-288.
- 631 [68] T. Martens, A. Bogaerts, J. van Dijk, *Appl. Phys. Lett.* 96 (2010) 131503.
- 632